UNIVERSIDADE DE SÃO PAULO

INSTITUTO DE FÍSICA
CAIXA POSTAL 20516
01498 - SÃO PAULO - SP
BRASIL

publicações

IFUSP/P-443

NUCLEAR STRUCTURE EFFECTS IN HEAVY-ION ELASTIC SCATTERING

by

Mahir S. Hussein
Instituto de Física, Universidade de São Paulo

Dezembro/1983

NUCLEAR STRUCTURE EFFECTS IN HEAVY-ION ELASTIC SCATTERING[†]

Mahir S. Hussein*

Instituto de Física, Universidade de São Paulo
C.P. 20.516, São Paulo, S.P., Brazil

ABSTRACT

Heavy-ion elastic scattering is discussed as containing two features; over all optical behavior characterized by several physical parameters such as the size of the system, the strength of the Coulomb interaction, etc., and deviations from this behaviour related directly to some aspects of the underlying nuclear structure. Two examples of such deviations are discussed in detail. The first is the anomalous back-angle scattering of nα-nuclei. The second example is connected with the effect of deformation.

[†]Based on lectures delivered at the VI Reunião de Trabalho sobre Física Nuclear no Brasil, Itatiaia, R.J., September 1983.

*Supported in part by the CNPq.

December/1983

I. INTRODUCTION

In discussing heavy-ion elastic scattering one usually emphasizes at length the wave optical behaviour. Such behaviour comes about as a result of several gross properties of the system. Its relatively large size, the strong absorption present (diffraction), strong Coulomb repulsion and nuclear attraction (refraction, rainbow and glory) and a well-defined surface region (determining the fall-off of $\frac{d\sigma}{d\Omega}$ in the shadow region). These features, quite common in most heavy-ion systems, constitute a convenient and useful "language" with which the elastic scattering may be described and analyzed.

Nuclei clearly exhibit other features besides the gross ones mentioned above. These other properties are more closely related to specific nuclear structure aspects, e.g., deformation. Therefore one would expect several important deviations from the optical behavior. Here, we shall discuss in detail two such deviations.

The paper is divided into two sections. The first, section II deals with the anomalous large-angle scattering of nα-nuclei. We shall concentrate on direct reaction interpretation of the anomalous behaviour and leave out completely intermediate structure resonance explanation. In section III we turn to the effect of nuclear deformation on $\frac{\sigma}{\sigma_R}$ at not too large energies. A convenient vehicle through which one may discuss the effect of the coupling to low-lying collective states is long-range absorption, which we shall discuss in detail.

II. ANOMALOUS BACK-ANGLE SCATTERING

A well-known case usually cited as exhibiting deviations from pure optical behaviour is that referring to systems behaving anomalously at back angles (α-scattering, $^{16}O + ^{28}Si$, etc.). What one usually discovers in these systems is a large increase in $\frac{\sigma}{\sigma_{Ruth}}(\theta)$ at back angles accompanied by a rather regular angular structure. Further, the excitation function $\frac{\sigma}{\sigma_{Ruth}}(\pi,E)$ at $\theta = \pi$ exhibits quite a conspicuous intermediate structure with an average width of about 1 MeV. To put the situation into perspective we show in Fig. 1 a plot

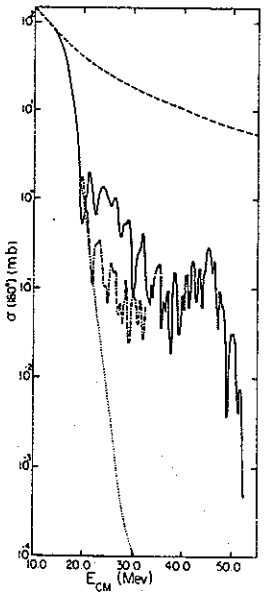

Fig. 1: Cross-sections at $\theta = 180^{o}$ vs. $E_{C.M.}$. Dashed line is the pure Coulomb elastic scattering cross-section for $^{16}O + ^{28}Si$. Dotted line is the cross-section obtained with the E-18 potential. Full curve is the experimental 180^{o}-excitation function for $^{16}O + ^{28}Si$, and dashed-dotted one for $^{16}O + ^{30}Si$.

of the experimental excitation function $\frac{d\sigma_{el}}{dr}(E,\pi)$ for $^{16}O + ^{28}Si$ and $^{16}O + ^{30}Si$. One sees clearly that the data sit at a mid-point between a pure Rutherford (no nuclear structure whatsover) and a pure strong absorption, E-18 (nuclear structure manifested purely optically).

Several interpretations have been advanced in the quest for a consistent description of the data. For a detailed discussion we refer the reader to the recent review by Braun-Munzinger and Barrette[2]. These interpretations range from a pure resonance, intermediate structure, picture affecting both the angular distributions and the excitation functions, to a pure-direct picture involving basically coupled channels feed-back-type effects. Neither of these extreme pictures seems to account for all facets of the data. Although recent measurements of angular distributions of α-transfer reactions, as well as inelastic scattering, of systems such as $^{16}O + ^{28}Si$ indicate that a pure, isolated resonance generated, intermediate structure interpretation of the gross structure of the anomalous back angle elastic scattering is not viable, owing to the lack of clear channels correlations, some type of resonancebased phenomenon is, however, certainly taking place and generating, at least the fine structure seen in most excitation functions.

Simple "direct" models have also been proposed for the purpose of explaining the gross features of the cross section at back angles. These range from simple changes in the "normal" optical potentials to simple changes in the "normal" elastic S-matrix. The necessity for invoking these changes in the normal "E-18" type description arose from two important observations; (a) the quite conspicuous rise in $\frac{\sigma}{\sigma_{Ruth}}(180^{o})$ to a value, at E_{cm} = 35 MeV, almost four orders of magnitude

bigger than the corresponding "E-18" value, and (b) the period of the angle oscillations, $\Delta\theta$, supplies a value of the contributing angular momentum $\ell_\theta(E)$ through $\Delta\theta \cong \frac{\pi}{\ell_\theta(E)}$, which is twice as large as the angular momentum, $\ell_E(E)$ that determines the period, ΔE, of the energy oscillation in the 180°-excitation function, $\Delta E \cong 1 / \frac{\partial \ell_E(E)}{\partial E}$.

The first anomaly has been accounted for through the use of the so-called surface transparent potentials. These optical potentials are characterized by an imaginary part with very small diffusiveness which results in an increased reflection. However, these potentials, though quite adequate in describing the angular distributions, fail dramatically in describing the second anomaly associated with the excitation function. This clearly points to the need for a second important modification of the normal optical E-18 potential, namely the addition of a small, albeit important parity-dependent component (proportional to $(-)^\ell$), which would not modify the angular distribution since it contributes mostly at back-angles. The 180° excitation function would then behave approximately $\sim \sin^2\left(\frac{\ell_E(E)}{2}\pi\right)$, thus giving rise to a local period $\Delta E = \frac{2}{\frac{\partial \ell_E(E)}{\partial E}}$, permitting the identification $\ell_\theta(E) = \ell_E(E)$. Ref. 3, exhibits the type of fit to the E-oscillations obtained by the Minnesota group with the above-mentioned two modifications in the optical potential describing $^{16}O + ^{28}Si$. A fit of a similar quality to the E-oscillations in the 180° excitation function was obtained in Ref. 4 using, as a starting point, the S-matrix description (Fig. 2). The elastic S-matrix used contains a normal optical E-18 type contribution, a parity-independent "window-like" contribution that peaks at an ℓ,

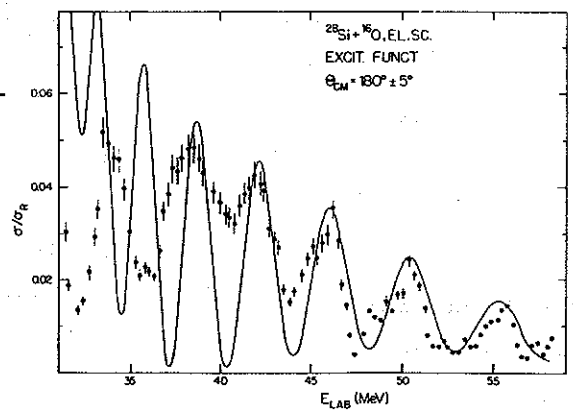

Fig. 2: Fit to the 180°-excitation function of $^{16}O + ^{28}Si$ obtained in Ref. 4.

slightly lower than the grazing one, and a small parity-dependent "window". The elastic S-element without the parity-dependent window was found to resemble very much the one generated from the surface transparent optical potential. The findings of Ref. 4 clearly support the conclusions reached by the Minnesota group concerning the need for a surface-transparent, parity-dependent optical potential.

A possible mechanism that gives rise to the anomalous behaviour of the heavy-ion system could be the coupling of the elastic channel to several important α-transfer channels. In the case of $^{16}O + ^{28}Si$, we may associate the parity independent window to the process depicted in Fig. (3). Similarly the parity dependent window can be attached to the diagram shown in Fig. (3c). This diagram does give rise to a $(-)^\ell$ term since

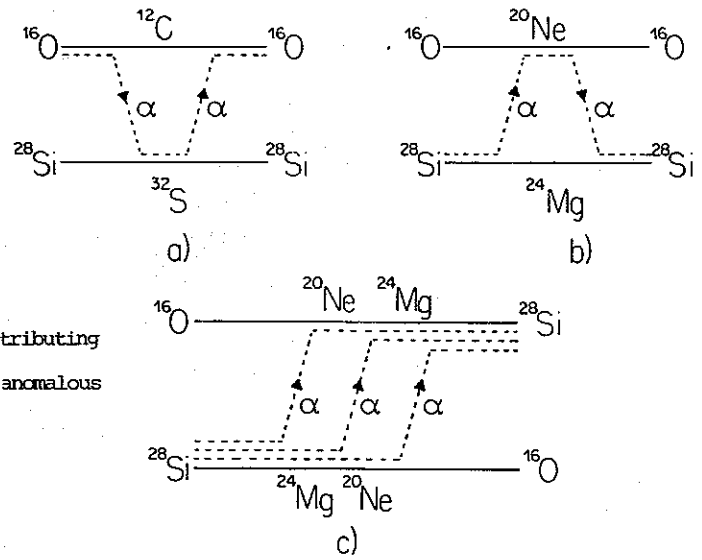

Fig. 3 - Contributing processes to anomalous scattering.

it represents an effective elastic transfer process.

We endeavour here to present a short account of how these diagrams generate ℓ and E windows.

The T-matrix representing the scattering in the elastic and α-transfer channels subspace may be given by

$$T = \overset{o}{T} + \tilde{\Omega}_o^{(+)} T' \Omega_o^{(+)} \tag{1}$$

where $\overset{o}{T}$ is diagonal and represents the "optical" E-18-type contribution, Ω_o is the corresponding Müller distorting operator

$$\Omega^o = 1 + G_o^{(+)} \overset{o}{T} \tag{2}$$

and T' is given by

$$T' = V + V G_o^{(+)} T' \tag{3}$$

and thus contributes to the transition. (V is assumed to be non-diagonal in channel space).

The elastic element of T may be generated perturbative

$$T = \overset{o}{T} + \Omega_o V \overset{o}{G}_t^{(+)} V \Omega_o^{(+)} + \Omega_o V \overset{o}{G}_t^{(+)} V \overset{o}{G}_o^{(+)} V \Omega_o^{(+)} \tag{4}$$

The second term corresponds to the diagram shown in Fig.(3a,b).

In order to exhibit the general characteristics of the contributing processes, we shall present a simple evaluation of these corrections based on the following approximations[5]

1) Consider only the on-shell part of $\overset{o}{G}_t$, $\overset{o}{G}_t \to -i\pi\delta(E_t - \overset{o}{H}_t)$

2) Use no-recoil.

The partial wave amplitude corresponding to a process of order n is then given by (ignoring angular momentum transfer)

$$(4\pi)^{2n+1} \prod_{j=n+1} \frac{1}{K_\ell(K_j, K_{j-1})} \prod_{j=1}^{n} \left[-i\pi \sqrt{\frac{\mu}{2(E-\varepsilon_j)\hbar^2}} \right] \cdot I_\ell(K_1, K) \prod_{j=1}^{n+1} [A_j] \tag{5}$$

where I_ℓ in the usual DWBA radial integral, K_ℓ is given by a corresponding integral involving the dual radial wave function ϵ_j the Q-value and A_j are spectroscopic factors. The K,s appearing in K_ℓ are bound state wave numbers. As shown in Ref. 5 the product $K_\ell I_\ell$ has a clear window shape whose details are determined by, among other things, the Sommerfeld parameter, and the K,s .

The elastic transfer diagram shown in Fig. (3c) can be evaluated along similar lines. Actually the fit obtained in Ref. (4) was partly tailored according to the description given above. The higher the order of the process,the narrower the resulting ℓ-window would be, as expected in any coherent multistep process.

The product KI also exhibits an energy-window shape[6]. To exhibit this characteristic of our anomalous transfer contribution to the elastic scattering T matrix, we use a semiclassical description of the transfer process, originally developed for the DWBA amplitude by Brink[7] and Broglia and Winther[8], and recently generalized to multistep transfer processes by Kammuri and Matsuoka[9]. The transition amplitude for a two-step sequential transfer via an intermediate state m is given by

$$C_{if}^{(2)} = (i\hbar)^{-2} \int_{-\infty}^{\infty} f_{mf}^{(1)}(t)\, dt \int_{-\infty}^{t} f_{im}^{(1)}(t')\, dt' \qquad (6)$$

where $f^{(1)}$ is the one-step form factor given by KM[9].

Specifying the intermediate state to be $^{12}C + ^{32}S$ and considering elastic scattering $f = i$, we obtain for $^{16}O + ^{28}Si$ [6]

$$C_{ii}^{(2)} = \frac{\pi N_1 N_2 R}{2i\hbar\bar{\gamma}} \left[1 + \frac{2}{i\sqrt{\pi}} F(x) e^{x^2} \right] \frac{1}{\Delta E} e^{-(0.23\Delta E + \frac{6.45}{\Delta E})} \qquad (7)$$

where

$x = \dfrac{2.54}{\sqrt{\Delta E}}$, F(x) is Dawson's integral

$\bar{\gamma} = \sqrt{\dfrac{2m_\alpha \bar{E}_\alpha}{\hbar^2}}$, N_1, N_2 are normalization consts.

, $\Delta E \equiv E - \bar{E} = E - 17.8$

In the above treatment absorption is not taken into account since it is implicitly assumed that one is considering only the grazing ℓ. We modify the above expression by considering the following estimate for the absorption

$$A = \exp\left[-\frac{2\mu}{\hbar^2} \int_{r_t}^{\infty} \frac{W_{E18}(r)}{k(r)} dr \right] \qquad (8)$$

when, as implied, W_{E18} is the imaginary part of the E-18 optical potential which is used rather widely to describe the elastic scattering of $^{16}O + ^{28}Si$ at small angles. The energy window associated with the round-trip α-transfer contribution to the elastic scattering is identified as the product $A\, C_{ii}^{(2)}$, which can be written as

$$A\, C_{ii}^{(2)} \cong \exp\left[-0.35\Delta E - 11.44\, (\Delta E)^{-1/2} \right] \qquad (9)$$

Figure (4) shows the result of applying Eq. (9) to the $^{16}O + ^{28}Si$ system, both for the parity-independent component of the anomalous E-window, Eq. (9) and the parity-dependent window $A\, C_{ii}^{(3)}$, with $C_{ii}^{(3)}$ calculated following the same procedure

as the one used for evaluating $C_{ii}^{(2)}$, Eq. (7)[6]. In both cases

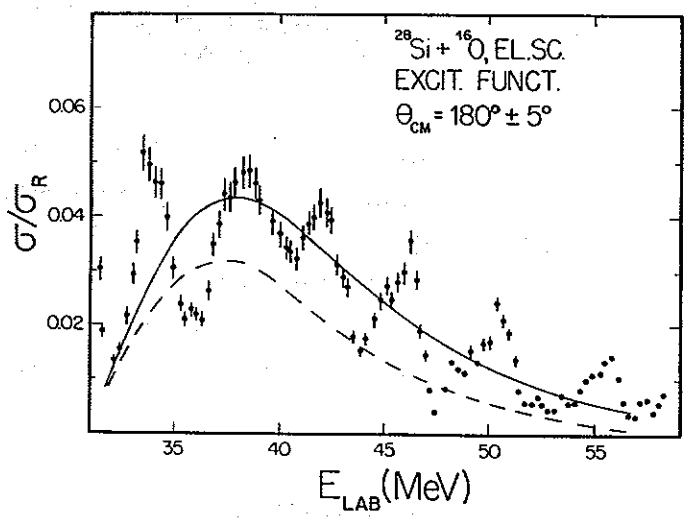

Fig. 4 - Energy windows calculated using Eq. (9). (From Ref. 6).

the same anomalous radius parameter, $\tilde{R} = 7.6$ fm (used previously in Ref. (4)) was employed.

As one can see the agreement of E_2 with the average trend of the excitation function data is quite good. The fine structure oscillations, according to our model, result from the interference between $A\,C_{ii}^{(2)}$ and $A\,C_{ii}^{(3)}$ (see Figs. (3a) and (3c)).

We should stress that there is no a priori reason that suggests the same value of $\tilde{r}_o$ for both $A\,C_{ii}^{(2)}$ and $A\,C_{ii}^{(3)}$. As a matter of fact it would seem more natural to take a smaller value for $\tilde{R}$ in $A\,C_{ii}^{(3)}$ than that in $A\,C_{ii}^{(2)}$ since the elastic transfer of three α,s is a higher order process than the round-trip process of one α. Furthermore

the data points themselves show that thre is a second major peaking at about $E_{cm} \cong 45$ MeV.

In Figure 5 we show our result using $\tilde{R}^{(2)} = 7.36$ fm and $\tilde{R}^{(3)} = 5.8$ fm.

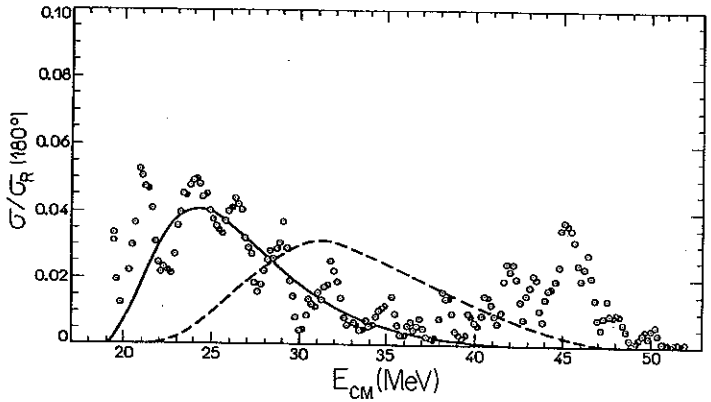

Fig. 5 - Same as Fig. 6, with two values of the anomalous radius.

We could not push the peaking of the $A\,C_{ii}^{(3)}$ to higher energies, as that would require the use of an anomalous radius at which W_{E-18} becomes quite large and a more exact treatment of A would be needed.

The sensitivity of our calculated window functions to the distance of closest approach of the corresponding transfer processes, is a possible indication that the anomalous back-angle data may furnish invaluable information concerning the ion-ion interaction at small separation distances. This fact is intimately related to the clear interplay between the

quasi-elastic, α-transfer processes, and the elastic scattering.

An important consequence of our findings is connected with the question of de-averaging the $180^{\circ} \pm 5^{\circ}$ - excitation function data addressed by Frahn and Kauffmann[10]. These authors correctly pointed out that as a result of the quite common procedure of averaging the data points in an angular interval $-5^{\circ} \leq \Delta\theta \leq 5^{\circ}$ around $\theta = 180^{\circ}$, one would necessarily end up with smaller over-all excitation function than the 180°-one. Clearly when confronted with dynamical models that supply a 180°-excitation function, the data has to be de-averaged.

We would like to point out at this point that this de-averaging procedure is model-dependent. It depends crucially on the value of critical radius attached to the mechanism responsible for the energy-structure in the excitation function. Therefore, in the light of our multi-step α-transfer model, the results of Ref. (10) have to be revised.

To show this, we first consider the results obtained by Frahn and Kauffmann[10]. The measured excitation function is an average of the differential cross section $\sigma(\theta)$ over a solid angle element $\Delta\Omega = 2\pi \sin\theta \Delta\theta$ with an interval $\Delta\theta = (\pi-\alpha, \pi)$, divided by the Rutherford cross section at $\theta = \pi$; this function will be denoted by $\bar{\rho}(E)$

$$\bar{\rho}(E) = \frac{1}{\Delta\Omega}\int_{\Delta\Omega} d\Omega \, \frac{\sigma(\theta,E)}{\sigma_R(\pi,E)} = \frac{1}{1-\cos\alpha}\int_{\pi-\alpha}^{\pi} d\theta \sin\theta \, \rho(\theta,E) \qquad (10)$$

It is clear that $\bar{\rho}$ can be evaluated if the angular dependence of $\rho(\theta,E) = \sigma(\theta,E)/\sigma_R(\pi,E)$ is known in $\Delta\theta$. It is known, however, that the enhanced large-angle scattering cross section has a universal structure given by

$$\rho(\theta,E) = G(\theta,E)\left[J_0(\tilde{\Lambda}\theta)\right]^2$$

$$\rho(\pi,E) = \rho(E) = G(0,E) \qquad (11)$$

where $G(\theta, E)$ is a slowly varying function of $\equiv \pi-\theta$ compared to the Bessel function $J_0(\tilde{\Lambda}\theta)$. The value $\tilde{\Lambda} = \tilde{\ell} + \frac{1}{2} >> 1$ denotes the anomalous angular momentum of the enhancement-causing part of the partial-wave S-matrix. It is related to the radius parameter through

$$\tilde{\Lambda} = k\tilde{R}\left(1 - \frac{\tilde{E}}{E}\right)^{1/2} \qquad (12)$$

where $\tilde{E}$ is the "threshold" of the anomaly, $\tilde{E} = 17.8$ MeV [6].

The de-averaging function $D(\alpha,E)$ defined by

$$D(\alpha,E) = \frac{\rho(E)}{\bar{\rho}(E)} = \left[\frac{1}{1-\cos\alpha}\int_0^{\alpha} d\theta \sin\theta \, \frac{G(\theta,E)}{G(0,E)}\left[J_0(\tilde{\Lambda}\theta)\right]^2\right]^{-1} \qquad (13)$$

can be evaluated in good approximation as

$$D(\alpha,E) = \left[\left[J_0(\tilde{\Lambda}\alpha)\right]^2 + \left[J_1(\tilde{\Lambda}\alpha)\right]^2\right]^{-1} \qquad (14)$$

The function $D(\alpha,E)$ is quite sensitive to the values of $\tilde{\Lambda}$ and accordingly $\tilde{R}$. To show this we exhibit in Fig. (6) the above function calculated with the two values of the anomalous radius referred to above $\tilde{R}^{(2)} = 7.36$ fm and

$\tilde{R}^{(3)} = 5.8$ fm.

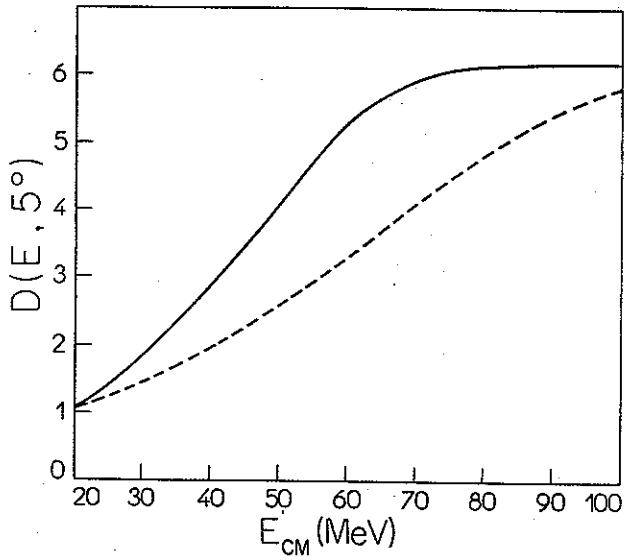

Fig. 6 – The de-averaging function $D(\alpha,E)$ calculated with $\tilde{R} = 7.36$ fm (full line) and $\tilde{R} = 5.8$ fm (dashed line).

By multiplying the data points of Ref. 2), in the energy range $20\ \text{MeV} < E_{cm} < 30\ \text{MeV}$ with $D(E,5^o)$ calculated with $\tilde{R}_1 = 7.36$ fm and the points in the energy range $30 < E_{cm} < 50$ MeV by $D(E,5^o)$ with $\tilde{R}_2 = 5.8$ fm (see Fig. 2), we obtain a de-averaged 180^o-excitation function that is more regular, with the second peaking at $E_{cm} = 45$ MeV attaining a value very close to the first major peaking at $E_{cm} \cong 23$ MeV. This is in contrast to the finding of Ref. 10) where there was a great disparity in favor of the second peaking.

It would be quite interesting to test the sensitivity of the de-averaging function to the anomalous radius experimentally by measuring averaged data for two different values of the averaging angle interval.

II. STATIC AND DYNAMIC DEFORMATION EFFECTS: LONG RANGE ABSORPTION

Another important case showing a clear deviation from the optical behaviour involves the scattering of deformed targets and/or projectiles at energies close to the Coulomb barrier. As a result of the strong Coulomb excitation of collective states, one expects a gradual depopulation of the elastic channel, even at sub-barrier energies. A nice example showing this effect is presented in Fig. 7 involving the system

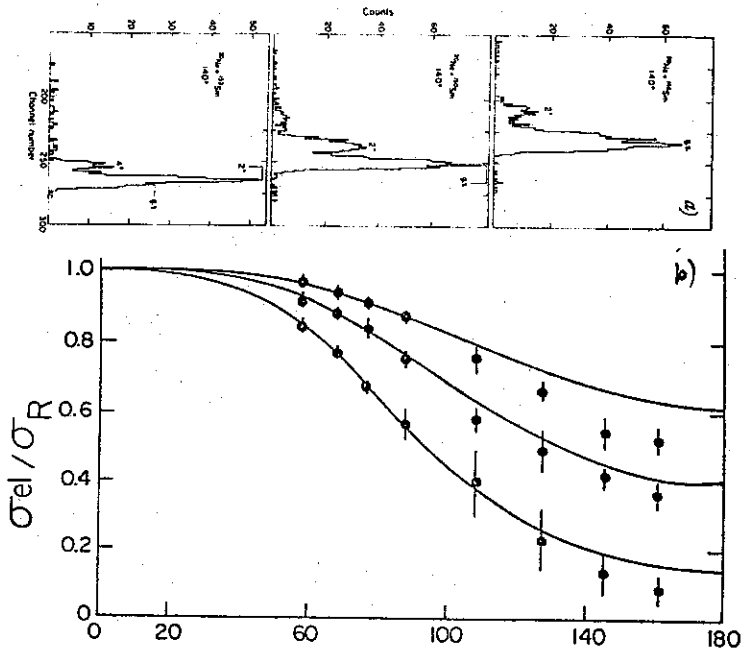

Fig. 7 – Spectra and $\frac{\sigma}{\sigma_R}$ for the system $^{16}O + {}^{A}Sm$. (From Ref. 11).

$^{20}Ne + {}^{A}Sm$, A = 148, 150 and 152 [11]. The strength of the coupling of the elastic 0^+ channel to the 2^+ state increases gradually from vibrational (^{148}Sm) to rotational (^{152}Sm), as is clearly seen in the ^{20}Ne-spectrum (Fig. (7.a)). Consequently the depopulation (absorption) in the $^{20}Ne + {}^{152}Sm$ is much stronger than either the $^{20}Ne + {}^{150}Sm$ and $^{20}Ne + {}^{148}Sm$. The cross-section ratio $\frac{\sigma(Ne + {}^{152}Sm)}{\sigma(Ne + {}^{148}Sm)}$ reaches its smallest value of ~0.2 at back angles.

The trend of the data clearly points to the presence of long-range absorption to be contrasted with the nuclear short-range absorption responsible for the diffractive behaviour discussed earlier. Actually the short range nuclear absorption, at the sub-barrier energies involved in the $^{20}Ne + {}^{A}Sm$ system under discussion, would give rise to a minor deviation from the Rutherford scattering, concentrated at angles very close to 180^{o}.

The long-range nature of the absorption referred to above cannot certainly be accounted for by a change in the optical potential, and one has to resort to coupled channels calculations. A more drastic departure from the optical behaviour, arising from the same coupled channels effect is shown in Fig. (8) [12]. The cm energy at which the data were taken is slightly above the Coulomb barrier of $^{18}O + {}^{184}W$, and then one would expect a conspicuous "Fresnel" form of $\frac{\sigma}{\sigma_{Ruth}}$ in the forward hemisphere. As one can clearly see the long-range absorption is quite strong even in this higher-energy case, resulting in a drastic modification of the "Fresnel" shape. Similar features are seen in the $^{12}C + {}^{184}W$ system at E_{Lab} = 70 MeV.

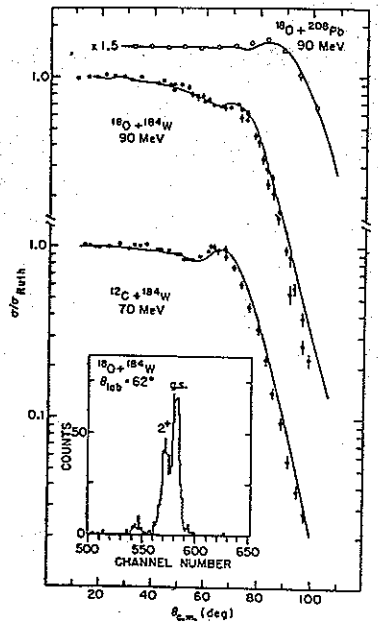

Fig. 8 - $\frac{\sigma}{\sigma_R}$ for $^{18}O + {}^{184}W$ at 90 MeV. (From Ref. 12). Also shown in $\frac{\sigma}{\sigma_R}$ for $^{18}O + {}^{208}Pb$ (90 MeV) and $^{12}C + {}^{184}W$ (70 MeV).

A way of simplifying the analysis of data such as the one above is through the construction of a component in the optical potential that represents the feed-back of the inelastic 2^+ channel into the elastic channel. This may easily be done through Feshbach's theory of the optical potential, which gives, in the particular case of two channels, the following form of the polarization potential

$$V_{pol.}(\vec{r},\vec{r}') = V_{02}(\vec{r})\, G_2^{(+)}(\vec{r},\vec{r}')\, V_{20}(\vec{r}') \qquad (15)$$

where $V_{02}(\vec{r})$ is the coupling potential and $G_2^{(+)}(\vec{r},\vec{r}')$ is the 2^+-channel Coulomb-modified Green's function.

When expanded in partial waves, the radial part of V_{pol}, would necessarily be angular momentum dependent and non-

local. However a locally-equivalent potential may be obtained approximately through the identification

$$\int V_{pol.}(\vec{r},\vec{r}')\,\psi_\ell(kr')\,dr' = V_{pol.}(r)\,\psi_\ell(kr) \tag{16}$$

where $\psi_\ell(k,r)$ represents the radial wave function in the elastic channel. At sub-barrier energies, $\psi_\ell(k,r)$ may be approximated by the regular Coulomb wave function $F_\ell(k,r)$, which makes possible the construction of $V_{pol}(r)$. The resulting expression for $V_{pol}(r)$ may be written as[13], ignoring the energy loss involved in the excitation process,

$$V_{pol.}(r) = -i\frac{2\pi}{25}\frac{\epsilon}{\eta}\frac{k^4}{\eta^2}\frac{B(E2)\uparrow}{Z_T^2 e^2}\left[\frac{3\bar{\ell}^2+1}{\bar{\ell}^2(\bar{\ell}+1)^2} - \bar{\ell}^{-3}\tan^{-1}\bar{\ell} + \frac{4\bar{\ell}^4}{(\bar{\ell}^2+1)^2}\frac{a}{r} + \frac{2\bar{\ell}^4}{(\bar{\ell}^2+1)^2}\frac{a^2}{r^2}\right]\left(\frac{a}{r}\right)^3 \tag{17}$$

$$\equiv -i\,\hat{V}_{pol}(r)$$

As a result of the assumption that the energy loss is zero $V_{pol}(r)$ comes out to be purely negative imaginary. The situation is reversed in the case of large energy losses, as $V_{pol}(r)$ becomes predominantly real. The reason is that in the former case the vibrational period is much larger than the collision time (sudden limit), therefore the system simply does not have enough time to react during the collision process and accordingly no modification are inflicted on the real interaction. In the large-energy-loss case (virtual excitation of giant resonances), the system manages to execute several vibrations during the collision process, thus resulting in a change in the effective real ion-ion interaction without inflicting much change in the absorptive component. For a detailed discussion on this point see Ref. (14).

The above long-ranged potential is a rather smooth

function of both ℓ and r. This feature permits the inclusion in $\frac{\sigma}{\sigma_{Ruth}}$ of the effect arising from the polarization potential in a simple manner. At energies below the Coulomb barrier the elastic scattering amplitude is dominated by the near-side Coulomb part. Accordingly only one turning point will contribute. Since owing to the fact that effect of long range absorption due to Coulomb excitation is mostly felt at not too high energies, one expects that the nearside amplitude dominates. Further, considering the polarization potential as a small perturbation, we may evaluate the resulting correction to the total phase shift using the WKB approximation

$$\delta_\ell = \overset{o}{\delta}_\ell - \frac{\mu}{\hbar^2}\int_{r_t(\ell)}^{\infty}\frac{V_{pol}(r)}{k_\ell(r)}\,dr \tag{18}$$

where $\overset{o}{\delta}_\ell$ is the "spherical" complex phase shift and $k_\ell(r)$ and $r_t(\ell)$ is the corresponding local wave number and turning point, respectively. Since $V_{pol}(r)$ is of a long range and acts in the interval $r_t(\ell) < r < \infty$, we may replace $k_\ell(r)$ and $r_t(\ell)$ by their Coulomb forms.

The stationary phase evaluation of the nearside amplitude $f_N(\theta)$ then yields

$$f_N(\theta) = \frac{1}{k\sqrt{\sin\theta}}\sum_i \left|\frac{\lambda_i}{\Theta'(\lambda_i)}\right|^{1/2} \exp\left[2i\delta(\lambda_i) - i\lambda_i\theta\right] \cdot \exp\left[-\frac{\mu}{\hbar^2}\int_{r_c(\ell_i)}^{\infty}\frac{|\mathrm{Im}\,V_{pol}(r)|}{k_{\ell_i}^c(r)}\,dr\right] \tag{19}$$

At sub-barrier energies, $\Theta(\lambda_i)$ may be considered predominantly Coulomb with a small correction arising from

$\mathrm{Re}\, V_{pol}(r)$,

$$\Theta(\lambda) = \Theta_{Ruth}(\lambda) - \frac{1}{E}\frac{\partial}{\partial b}\left[\frac{1}{b}\int_0^{\phi_0} r^2\, \mathrm{Re}\, V_{pol.}(r)\, d\phi\right] \qquad (20)$$

where $\phi_0 = \tan^{-1}\frac{b}{a}$

Our one-stationary-phase-point approximation for $\frac{d\sigma}{d\Omega}$, then reads

$$\frac{d\sigma}{d\Omega} = \frac{b}{\sin\theta}\left|\frac{db}{d\theta}\right| \exp\left[-\frac{2\mu}{\hbar^2}\int_{r_c^\ell}^{\infty} \frac{|\,\mathrm{Im}\, V^{\ell}_{pol.}(r)\,|}{k^c_\ell(r)}\, dr\right] \qquad (21)$$

which, upon evaluating b and $\frac{db}{d\theta}$ to first order in $\Delta\theta$, can be cast into the following

$$\frac{\sigma}{\sigma_{Ruth}}(\theta) = \left[1 + \frac{1}{2}\Delta\theta \tan\frac{\theta}{2} + \frac{3}{2}\Delta\theta \cot\frac{\theta}{2} - \frac{d}{d\theta}\Delta\theta\right] \cdot$$

$$\cdot \exp\left[-\frac{2\mu}{\hbar^2}\int_{r_c}^{\infty} \frac{|\,\mathrm{Im}\, V^{\ell}_{pol.}(r)\,|}{k^c_\ell(r)}\, dr\right] \qquad (22)$$

The above formula was found to be quite adequate in describing sub-barrier elastic scattering of heavy ions. For strongly deformed nuclei the inclusion of the low lying 2^+

state in evaluating V results in a almost purely absorptive polarization potential. The correction $\Delta\theta$ due to the real component is quite negligible. Using V' of Eq. (17), then results in

$$\frac{\sigma}{\sigma_{Ruth}}(\theta) = \exp\left[-\frac{16}{45}\, q^2\, g(\theta)\right] \quad ,$$

$$q^2 = \frac{\pi}{5}\frac{k^4}{\eta^2}\left[\frac{B_T(E2)\, g_T(\xi_T)}{Z_T^2 e^2} + \frac{B_p(E2)\, g_p(\xi_p)}{Z_p^2 e^2}\right] \quad , \qquad (23)$$

$$g(\theta) = \frac{9}{4}\left[\frac{1}{3}\left(\sin\frac{\theta}{2}\right)^4 + \left(\tan\frac{\theta}{2}\right)^4\left(1 - \left(\tan\frac{\theta}{2}\right)\frac{1}{2}(\pi-\theta)\right)^2\right] .$$

The angular function $g(\theta)$ attains its maximum value of unity at $\theta = \pi$, and it vanishes at $\theta = 0$. The solid lines in Fig. (7a) are simply the $\frac{\sigma}{\sigma_{Ruth}}$ of Eq. (23) calculated after approximately accounting for the small energy-loss encountered in $^{20}Ne + {}^{A}Sm$, through the quantities $g_T(\xi_T)$ and $g_p(\xi_p)$ with $\xi = \frac{1}{2}\,\eta\,\frac{\Delta E}{E}$ (see Refs. 13 and 14).

In the other extreme of scattering of spherical nuclei where Coulomb excitation of low-lying states is negligible, the virtual excitation of giant resonances come into play. Here the adiabatic limit gives a purely <u>real</u> ℓ-independent polarization potential which has the following form for the giant quadrupole case

$$V^{(2)}_{ad.\,pol.}(r) = -\frac{4\pi}{25}\left[Z_p^2 e^2 \frac{B_T(E2)\uparrow}{\Delta E_T^{(2)}} + \frac{Z_T^2 e^2\, B_p(E2)\uparrow}{\Delta E_p^{(2)}}\right]\Big/ r^6$$

$$\equiv V_o^{(2)}\Big/ r^6 \qquad (24)$$

where ΔE is the excitation energy of GQR ($\Delta E^{(2)} \sim \frac{60}{A^{1/3}}$ MeV) and B(E2) is the corresponding reduced excitation probability.

When used in Eqs. (6) and (8), we obtain the following expression for $\frac{\sigma}{\sigma_R}$ [15]

$$\frac{\sigma}{\sigma_{Ruth}} = 1 - \frac{V_0^{(2)}}{8Ea^6}\frac{\cos^6\phi_0}{\sin^{10}\phi_0}\left\{\left[-\frac{3}{2}\tan\phi_0 - \frac{9}{2}\cot\phi_0\right]\cdot\right. \tag{25}$$

$$\cdot\left[-315\phi_0 + 420\phi_0\sin^2\phi_0 - 120\phi_0\sin^4\phi_0 \cdot\right.$$

$$\left. + 315\cos\phi_0\sin\phi_0 - 210\cos\phi_0\sin^3\phi_0 + 8\cos\phi_0\sin^5\phi_0\right]$$

$$+\frac{1}{2}\left[840\phi_0\sin\phi_0 - 480\phi_0\sin^3\phi_0\cos\phi_0\right.$$

$$\left. - 84\cdot\sin^2\phi_0 + 960\sin^4\phi_0 - 48\sin^6\phi_0\right]\Big\}.$$

Though quite small, the deviation from unity of $\frac{\sigma}{\sigma_{Ruth}}$ due to the virtual GQR excitation together with other small effects, has been observed recently by Lynch et al.[16].

Although we have presented our expression for $\frac{\sigma}{\sigma_R}$, Eq. (23), that correspond to the case of one real stationary phase point, adequate at sub-barrier energies, the generalization to above barrier energies is quite simple. This comes about as a result of the rather slow ℓ-dependence of $V_{pol}(r)$, which even in cases involving two stationary phase points, i.e. Coulomb rainbow scattering or Fresnel diffraction, can be factored out as a common factor to both contributions. This is particularly valid near the rainbow angle (or critical Fresnel angle). Therefore we may write in general

$$\frac{d\sigma}{d\sigma_{Ruth}}(\theta) = \left(\frac{\sigma}{\sigma_{Ruth}}(\theta)\right)_0 \exp\left[-\frac{16}{45}q^2 g(\bar{\ell}(\theta))\right], \tag{26}$$

where $\bar{\ell}$ corresponds to the average value of the two stationary phase angular momenta. To show the adequacy of the above description we show in figure (9) the calculation of $\frac{\sigma}{\sigma_{Ruth}}$ for $^{16}O + ^{184}W$ at $E_L = 90$ MeV done both though optical model calculation that included V_{pol} and the result obtained from Eq. (26) with $\left(\frac{\sigma}{\sigma_{Ruth}}\right)_0$ calculated with an optical potential that does not contain V_{pol}. The agreement is very good.

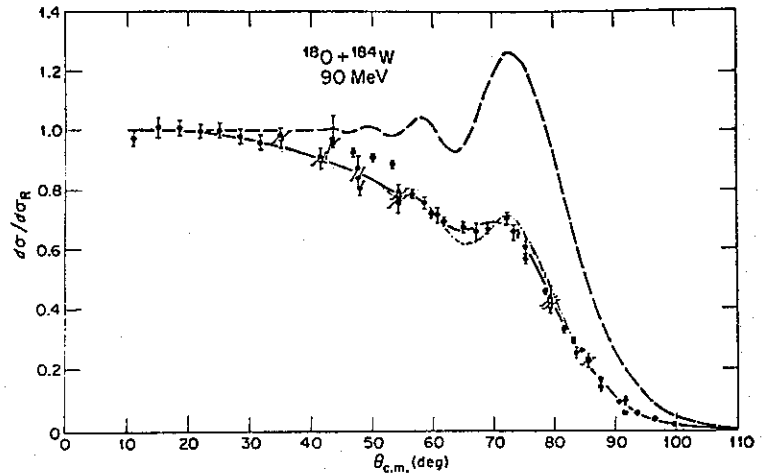

Fig. 9 - Dashed curve is $\left(\frac{\sigma}{\sigma_R}\right)_0$ (Eq. 26) obtained with the optical potential, V = 40 MeV, W = 9.06 MeV, r_o = 1.313 fm and a = 0.457 fm. Full curve is obtained when V_{pol} is added to the potential above. [From W.Love et al., Phys. Rev. Lett. 39 (1977) 6. The dashed-dotted curve is the result obtained from Eq. (26).

REFERENCES

1) See, e.g., M.S. Hussein and K.W. McVoy, "Heavy Ion Optics in the Near/Far Representation", Progress in Particle and Nuclear Physics, in press.

2) P. Braun-Munzinger and J. Barrette, Phys. Rep. C87 (1982) 209.

3) D. Dehnhard et al., Phys. Rev. Lett. 40 (1978) 549; erratum, Phys. Rev. Lett. 42 (1979) 1574.

4) W.E. Frahn et al., Nucl. Phys. A369 (1981) 166.

5) W.E. Frahn and M.S. Hussein, Nucl. Phys. A346 (1980) 237.

6) L.F. Canto et al., Phys. Rev. Lett. 51 (1983) 95.

7) D.M. Brink, Phys. Lett. 40B (1972) 37.

8) R. Broglia and A. Winther, Phys. Rep. 4C (1972) 153.

9) T. Kammuri and K. Matsuoka, Nucl. Phys. A366 (1981) 171.

10) W.E. Frahn and K. Kauffmann, Phys. Rev. C (1982).

11) P. Doll et al., Phys. Lett. 76B (1978) 566.

12) C.E. Thorn et al., Phys. Rev. Lett. 38 (1977) 384.

13) A.J. Baltz et al., Phys. Rev. Lett. 40 (1978) 20; Nucl. Phys. 327A (1979) 221.
R. Donangelo et al., Nucl. Phys. 320A (1979) 422.

14) A.J. Baltz, M.S. Hussein and B.V. Carlson. To appear in Phys. Rep.

15) A.J. Baltz and M.S. Hussein, Phys. Lett. 132B (1983) 274.

16) W.G. Lynch et al., Phys. Rev. Lett. 48 (1982) 979.